Published in final edited form as:
Science. 2011 April 15; 332(6027): 322–327. doi:10.1126/science.1202793.

Structure of an agonist-bound human A_{2A} adenosine receptor

Fei Xu[1], **Huixian Wu**[1], **Vsevolod Katritch**[2], **Gye Won Han**[1], **Kenneth A. Jacobson**[3], **Zhan-Guo Gao**[3], **Vadim Cherezov**[1], and **Raymond C. Stevens**[1,*]

[1]Department of Molecular Biology, The Scripps Research Institute, 10550 North Torrey Pines Road, La Jolla, CA 92037, USA

[2]Skaggs School of Pharmacy and Pharmaceutical Sciences and San Diego Supercomputer Center, University of California, San Diego, La Jolla, CA 92093, USA

[3]Laboratory of Bioorganic Chemistry, National Institute of Diabetes & Digestive & Kidney Diseases, National Institutes of Health, Bethesda, MD 20892, USA

Abstract

Activation of G protein-coupled receptors upon agonist binding is a critical step in the signaling cascade for this family of cell surface proteins. Here we report the crystal structure of the A_{2A} adenosine receptor (A_{2A}AR) bound to an agonist UK-432097 at 2.7 angstrom resolution. Relative to inactive, antagonist-bound A_{2A}AR, the agonist-bound structure displays an outward tilt and rotation of the cytoplasmic half of helix VI, a movement of helix V and an axial shift of helix III, resembling the changes associated with the active-state opsin structure. Additionally, a seesaw movement of helix VII and a shift of extracellular loop 3 are likely specific to A_{2A}AR and its ligand. The results define the molecule UK-432097 as a "conformationally selective agonist" capable of receptor stabilization in a specific active state configuration.

G protein-coupled receptors (GPCRs) are critical cellular signal transduction gatekeepers for eukaryotic organisms, both through the activation (agonists) and inactivation (inverse agonists and antagonists) of the receptors using a variety of different ligands. Recent breakthroughs on elucidating crystal structures of GPCRs bound to diffusible ligands include five class A GPCRs: β_2 (1-7) and β_1 (8,9) adrenergic receptors, A_{2A} adenosine receptor (A_{2A}AR) (10), CXCR4 chemokine receptor (11) and D3 dopamine receptor (12). All structures confirm a common seven transmembrane (7TM) topology for GPCRs, as well as substantial variations in functionally divergent regions, especially on the extracellular side of the receptor responsible for recognition of a vast variety of ligands. To overcome the challenge of crystallizing highly dynamic GPCRs, each of these receptors were engineered to increase their stability and were co-crystallized with stabilizing ligands.

The mechanism of GPCR activation by native ligands (or synthetic agonists), however, is a fundamental question that remains largely unsolved. An initial model for GPCR activation was provided by the crystal structures of retinal-free opsin (13,14), but the absence of any agonist precludes direct generalization of this result to other GPCRs activated by diffusible ligands. To shed light on the mechanism of ligand-induced GPCR activation, we have determined a 2.7 Å crystal structure of the human A_{2A}AR in complex with the A_{2A}AR agonist 2-(3-(1-(pyridin-2-yl)piperidin-4-yl)ureido)ethyl-6-N-(2,2-diphenylethyl)-5′-N-

*To whom correspondence should be addressed: stevens@scripps.edu .

Changes associated with conformationally selective agonist binding shed light on G protein-coupled receptor activation.

Supporting Online Material www.sciencemag.org Materials and Methods Tables S1 to S3 Figs. S1 to S4 References Movie: A_{2A}AR activation transition

ethylcarboxamidoadenosine-2-carboxamide (UK-432097). This highly potent and selective agonist, which was developed as a drug candidate for COPD (Chronic Obstructive Pulmonary Disease) treatment (15), represents a substituted derivative of the native ligand adenosine and a series of other prototypical adenosine receptor (AR) agonists, e.g. NECA, CGS21680, ATL-146e and CI-936 (16-18). The availability of both agonist- and antagonist-bound A_{2A}AR structures now provides the opportunity to understand the basic question of how ligand binding at the extracellular side of the receptor triggers conformational changes at the intracellular side where G protein and other effectors bind and initiate the cascade of downstream signaling pathways.

Agonist UK-432097 and its binding cavity

The compound UK-432097 was characterized as a full A_{2A}AR agonist (19), (20) (fig. S1 and S2 (21)) and its structure in complex with human engineered A_{2A}AR (A_{2A}AR-T4L-ΔC) was determined similarly to A_{2A}AR-T4L-ΔC bound to the antagonist ZM241385 at 2.7 Å resolution (10), (22)(table S1). UK-432097 (778 Daltons) is more than twice as large as ZM241385 and occupies most of the A_{2A}AR ligand-binding cavity (Fig. 1A and fig. S3). The ligand-binding cavity reveals an extensive ligand-receptor interaction network, including 11 hydrogen bonds, one aromatic stacking interaction and a number of non-polar (van der Waals) interactions (Fig. 1B and table S2). These interactions explain the high binding affinity and subtype selectivity of this compound and its strong stabilizing effect on A_{2A}AR (table S3).

The bicyclic *adenine core* of UK-432097 is a common scaffold and present in nearly all major types of AR agonists (e.g. NECA, CGS21680, and other nucleosides) and many antagonists (23). This moiety aligns to the triazolotriazine core of ZM241385 when the two complex structures are superimposed together (Fig. 1A), as predicted in modeling studies (24,25). The molecular interactions that anchor ZM241385 in this region are also conserved in the UK-432097 binding cavity, including aromatic stacking with Phe168 in extracellular loop 2 (ECL2), non-polar interaction with Ile274$^{7.39}$, and two hydrogen bonds with Asn253$^{6.55}$ (26)(27) (Fig. 1C). Significant effects are observed on mutation of these residues on both agonist and antagonist binding: Phe168 (moderate decrease), Ile274$^{7.39}$ (major decrease), or Asn253$^{6.55}$ (complete loss) (25,28).

The *ribose ring* is a key feature of almost all known AR agonists that differentiates them from corresponding antagonists. In the A_{2A}AR/UK-432097 complex, the ribose moiety of the ligand inserts deeply into a predominantly hydrophilic region of the binding cavity (Fig. 1), with the 2′ and 3′ –OH groups both making hydrogen bonds with His278$^{7.43}$ (2.8 Å and 3.1 Å, table S2). The 3′ –OH is further anchored by a hydrogen-bonding interaction with Ser277$^{7.42}$ (3.0 Å) (Fig. 1D). Mutation of these two residues to alanine abolishes high affinity binding of A_{2A}AR agonists (28). His250$^{6.52}$ forms a hydrogen-bonding interaction with the carbonyl O4 (3.1 Å) that was not predicted in agonist docking to inactive states of the ARs. Mutation to alanine or phenylalanine disrupts agonist binding indicating this residue is important for agonist recognition (29). The ribose 5′-*N*-ethyluronamide substitution in UK-432097, as well as in NECA and many other AR agonist chemotypes, is known to provide additional potency. The N2 of this moiety makes a hydrogen bond with Thr88$^{3.36}$ (3.0 Å), in accord with reduction in binding observed for the T88A mutant of A_{2A}AR (30). Besides these polar interactions, the ribose part of the ligand has close contacts with Val84$^{3.32}$, Leu85$^{3.33}$, Trp246$^{6.48}$, Met177$^{5.38}$ and Leu249$^{6.51}$. Previous mutagenesis data on V84A or L249A suggested these non-polar interactions are essential for agonist binding (25,29).

The bulky 2-(3-(1-(pyridin-2-yl)piperidin-4-yl)ureido)ethylcarboxamido substitution in UK-432097 is located at the adenine C2 position; similar extended chains are found in many of the selective A_{2A}AR agonists under development (15). The carboxamide moiety forms an indirect water-mediated hydrogen bond with Tyr9$^{1.35}$ and the carbonyl group of Ala63$^{2.61}$, which contributes to a closer contact of the ligand with helices I and II (Fig. 1E). The urea group is coordinated on both sides by Glu169 (ECL2) forming two hydrogen bonds at N8 and N9 positions (2.8 Å and 2.7 Å) and Tyr271$^{7.36}$ forming one hydrogen bond at O6 (2.7 Å). Finally, the pyridinyl-piperidine moiety leans to the two phenyl rings and bulges toward helix VII and ECL3. This combined moiety might impose an allosteric effect on structural and conformational changes of the receptor and contribute to subtype binding selectivity (18,31-33).

Antagonist-bound to agonist-bound transformations in A_{2A}AR

Changes in ligand binding cavity

A comparison of the A_{2A}AR complexes with antagonist ZM241385 and agonist UK-432097 shows that while the core adenine interactions are conserved between the two structures, binding of the agonist UK-432097 triggers a series of conformational changes within the binding cavity of A_{2A}AR (Fig. 2). Importantly, some of these modest local changes promote large-scale rearrangements in the 7TM helical bundle (Fig. 3). The specific molecular interactions with the ribose moiety of UK-432097 are likely a common feature for all A_{2A}AR agonists, with motions of the ribose-coordinating residues related to the receptor activation. In helix VI, for example, His250$^{6.52}$ moves ~1.8 Å inward to a position that would otherwise clash with the furan ring of ZM241385 and forms a hydrogen bond with the carbonyl group (Fig. 1D and fig. 2A). The conserved Trp246$^{6.48}$ indole moves ~1.9 Å to avoid a steric clash with the ribose ring of the agonist, a movement that facilitates rotation and tilt of the intracellular side of helix VI below Pro248$^{6.50}$. Although helix V residues Met177$^{5.38}$, Asn181$^{5.42}$ and Val186$^{5.47}$ make only limited non-polar contacts with the agonist, the movement of His250$^{6.52}$ allows an inward shift of Val186$^{5.47}$, promoting an inward tilt of the whole intracellular side of helix V (Fig. 2A).

In helix VII, Ser277$^{7.42}$ and His278$^{7.43}$ move about 2 Å closer to helix III and together with the side chain of Thr88$^{3.36}$ form a hydrogen-bonding network coordinating the ribose moiety (Fig. 1D and fig. 2A). Two residues on the extracellular end of helix VII, Leu267$^{7.32}$ and Met270$^{7.35}$, form additional non-polar interactions with the two phenyl rings and piperidine rings of UK-432097, resulting in an outward movement of these two residues along with the extracellular part of helix VII by about 2 Å (Fig. 2B). The motion of the helix VII apex correlates with an even more pronounced (3-4 Å) outward movement of the adjacent ECL3 backbone, where the His264 imidazole swings by 100° from beneath the pyridine ring to the top of the ligand-binding cavity (Fig. 2B). Also, Glu169 (ECL2) has a different rotamer conformation than in the A_{2A}AR/ZM241385 structure, where its carboxylic group forms a hydrogen bond with the exocyclic amine of ZM241385. Due to a substitution in the exocyclic amino group of UK-432097, the Glu169 carboxyl group moves about 4 Å to form hydrogen bonds with the urea substituent instead, coordinating both the urea group and the two phenyl rings in position. The latter two changes in ECL3 and ECL2 largely depend on substituted moieties in the agonist and are likely to be specific for UK-432097 or agonists with similar bulky substitutions.

In helix III, coordination of the ribose ring through hydrogen bonding interaction with Thr88$^{3.36}$ side chain, as well as non-polar contacts with Val84$^{3.32}$ and Leu85$^{3.33}$, requires a ~2 Å shift of these residues, resulting in an upward shift of the entire helix III along the helical axis (Fig. 2A and Fig. 3A).

Rearrangement within 7TM bundles

Comparison of this A_{2A}AR-agonist complex structure to its antagonist-bound form shows that helices I-IV form a stable helical bundle "core" with minimal structural changes, while helices V-VII undergo substantial conformational changes (34). The movements are illustrated in Fig. 3A-D by graphical superimposition of the two protein conformations (using Cα atoms of TM helices), as well as by plotting full residue RMSDs (root mean square deviations; shown on Y axis) and deviations of Cα atoms (shown by color) for individual residues in Fig. 3E. This "RMSD fingerprint" representation conveniently differentiates side-chain rotameric switches (green-blue colored outliers, marked by residue labels) and global motions of helices (clusters of yellow-red dots).

One of the most prominent changes associated with the agonist-bound structure involves coordinated movements of the intracellular parts of helices VI and V. While the extracellular part of helix VI is fixed in place by the key interactions of Asn253$^{6.55}$ with the exocyclic amino group of UK-432097, the agonist-induced shift of the conserved Trp246$^{6.48}$ promotes an outward tilt of the intracellular part of helix VI by about 3-4 Å and clockwise rotation by about 30 deg. (Fig. 3). The shift of helix VI is accompanied by coordinated rotameric switches in Phe201$^{5.62}$ and Tyr197$^{5.58}$ side chains. While in A_{2A}AR/ZM241385 the conserved Tyr197$^{5.58}$ is placed in the middle of the helical bundle between helices III and VI, in the UK-432097-bound form this residue moves outward allowing helix V shift toward helix VI. As a result of this combined tilt, the intracellular ends of helices V and VI move closer together in the A_{2A}AR/UK-432097 structure (~6 Å) as compared to the A_{2A}AR/ZM241385 structure (~8 Å) (Fig. 3D).

Another response to the binding of the agonist UK-432097 is a seesaw-like movement of helix VII around the ribose ring. While interactions of the ribose ring hydroxyls with Ser277$^{7.42}$ and His278$^{7.43}$ pull these residues of helix VII inwards, strong clashes of the two phenyl rings with Leu267$^{7.32}$, Met270$^{7.35}$, Tyr271$^{7.36}$ and ECL3 residues push the extracellular part of helix VII outwards, creating a lever that promotes a tilt of helix VII. The conserved NPxxY motif composed of Asn284$^{7.49}$, Pro285$^{7.50}$, Phe286$^{7.51}$, Ile287$^{7.52}$ and Tyr288$^{7.53}$ at the cytoplasmic end of helix VII shifts as much as 4-5 Å inwards, resulting in reorganizations of these side chains, especially Tyr288$^{7.53}$ (Fig. 3, also Fig. 4 A and C).

Insight into a GPCR activation mechanism

The conformational changes observed between the A_{2A}AR-agonist and A_{2A}AR-antagonist complexes can be further understood in the context of comparison with the structural transitions in the light-activated rhodopsin/opsin system (13,14). Unliganded opsin at low pH adopts a conformation similar to the light-activated rhodopsin at physiological pH (35). Concomitant structural transitions between the inactive rhodopsin and active-like opsin include side-chain switches in the conserved D[E]RY and NPxxY motifs and rearrangements of helices V-VII. Structural superimposition along with "RMSD fingerprint" of individual residues between the two pairs of models: inactive/active A_{2A}AR structures and rhodopsin/opsin structures reveals considerable similarity attributed to a general GPCR activation mechanism (Fig. 4).

The RMSD fingerprint plots shown in Fig. 4D for both inactive/active pairs (rhodopsin/opsin and A_{2A}AR-antagonist/A_{2A}AR-agonist) of TM domains illustrate similarities between the conformational transitions in these two different receptor systems. For example, a similar pattern is observed of very low deviations in helices I, II and IV, and of elevated backbone deviations in helices III, V and VI (Correlation Coefficient between two sets of RMSDs R^2=0.64 for helices I to VI, and R^2=0.84 for helix VI alone). In contrast, the plot suggests a lack of similarity in helix VII (R^2=0.25 for helix VII alone).

The predominant feature common between opsin and $A_{2A}AR$ is the overall movement of helices V and VI, with their extracellular parts being the least mobile and intracellular parts deviating dramatically. The conserved $Trp^{6.48}$ is an important residue triggering the motion of helix VI during activation in $A_{2A}AR$, however, contrary to previous "toggle switch" model, this residue does not undergo a rotamer transition, but rather moves along with the backbone in both opsin and $A_{2A}AR$. The overall backbone shifts in both opsin and $A_{2A}AR$ are accompanied by rotameric switches of $Tyr^{5.58}$, however the observed changes in this residue upon activation are very different – while in opsin this side chain swings from outside toward the axis of the TM bundle, the movement in $A_{2A}AR$ is the opposite (36). Also, rotameric changes in non-conserved rhodopsin side chains $Phe^{5.55}$ and $Phe^{5.43}$ were not observed in the same positions of $Leu^{5.55}$ and $Phe^{5.43}$ in $A_{2A}AR$.

Another characteristic molecular switch in rhodopsin/opsin activation model is a salt bridge (so called ionic lock) between $Arg^{3.50}$ of the conserved D[E]RY motif in helix III and $Glu^{6.30}$ in helix VI. The ionic lock breaks in opsin upon activation resulting in rotameric changes in $Glu^{6.30}$ and movement of helix VI away from helix III (Fig. 4A). While the ionic lock is already broken in $A_{2A}AR$-antagonist structure (10), the concerted movements of helices III and VI observed in the $A_{2A}AR$/UK-432097 complex also pull $Arg102^{3.50}$ and $Glu228^{6.30}$ further apart, precluding any potential interactions between these residues. A noteworthy difference in this region is that while in our $A_{2A}AR$-agonist complex structure the middle segment of the cytoplasmic half of helix VI bulges outward by ~3-4 Å, the movement of the intracellular tip of helix VI is not as pronounced as in opsin (~3 Å vs. 6-7 Å, Fig. 4A). However, such partial "attenuation" of the outward tilt of helix VI in this structure may be attributed to the fused T4 lysozyme (T4L), which is likely to limit mobility of the cytoplasmic ends of helices V and VI.

A third featured transition that may be related to activation is a ~2 Å movement of helix III in the context of the overall well-preserved helices I-IV bundle "core" (37). The movement that involves helix III sliding along its axis toward the extracellular side, can be found in both rhodopsin/opsin and $A_{2A}AR$ systems; in the case of the $A_{2A}AR$/UK-432097 complex it allows formation of new contacts with the ribose ring of the agonist.

Conformational changes in helix VII also reveal both common and distinct features for $A_{2A}AR$ and rhodopsin/opsin (Fig. 4). One common feature is a large-scale (>5 Å) movement and rotameric switch of the $Tyr^{7.53}$ side chain in the highly conserved NPxxY motif at the intracellular tip of helix VII. In the $A_{2A}AR$-agonist structure, however, the $Tyr288^{7.53}$ movement is coordinated by a dramatic rigid body tilt of helix VII, so that the Cα atoms in this region move more than 5 Å. Conversely, in opsin the backbone of helix VII does not move overall, while movement of $Tyr^{7.53}$ is achieved via local bulging of the backbone in this region. This conformational change in $Tyr^{7.53}$ has been implicated in the activation mechanism of rhodopsin and other GPCRs, and is likely to be important for the transition from the inactive to active state in $A_{2A}AR$ (14,38-40). Note that while the changes described above in $A_{2A}AR$ helices III, V, VI, and VII have a major component of "rigid body" movement, a more detailed analysis shows certain conformational plasticity of the helices. In other words, rather than being "rigid sticks", the movements of TM helices are more consistent with elastic spring behavior (see fig. S4 for details).

Recently, agonist-bound structures of β_1- and β_2- adrenergic receptors (β_1-/β_2ARs) have been reported (2,5,9). The β_1AR structures (9) and the structure of β_2AR bound to an irreversible agonist (5) highlighted important conformational changes in the orthosteric binding site, but did not exhibit agonist-induced conformational changes at the intracellular side of these receptors. The pseudo active-like state conformation in β_2AR with intracellular conformational changes was achieved by additional stabilization of an agonist–bound

receptor with a G-protein mimicking nanobody (2). The nanobody-stabilized agonist-bound β_2AR structure revealed large-scale movements of helices III, V, VI and VII along with rotamer switches of conserved residues at the cytoplasmic G-protein binding interface, similar to those observed in the activated opsin and in the current agonist-bound A_{2A}AR structure. Some variations in the magnitude of these movements may be partially explained by intrinsic differences between these three receptors, as well as by specific effects of the receptor binding partners. For example, a larger magnitude of helix VII movement in A_{2A}AR may result from conformational changes specific for the bulky UK-432097 ligand, while the magnitude of helix VI movement in β_2AR may be exaggerated by the nanobody binding. Despite the similar conformational transformations occurring at the intracellular side of the agonist/nanobody stabilized-β_2AR and agonist bound A_{2A}AR, these changes appeared to be induced by rather disparate triggers associated with agonist binding in different receptors. Ligand-induced activation in β_2AR is largely driven by an inward movement of helix V (2,41), while binding of A_{2A}AR agonist does not directly affect helix V, instead the most pronounced ligand-induced changes involve helices III, VI and VII.

The observed resemblance in the overall structural rearrangements in the A_{2A}AR, opsin and β_2AR suggests common features of activation mechanism in GPCRs (Fig. 5). While agonist binding at the extracellular domain triggers only subtle conformational changes within the binding pocket, some of these changes propagate toward the cytoplasmic domains promoting large-scale 7TM rearrangement required for G-protein binding and signaling. Movements on helices V-VII are supported by a relatively stable core bundle composed of helices I-IV. Comparison of activation transitions in A_{2A}AR, opsin and β_2AR reveals very different types of molecular triggers in the binding pocket, which promote or stabilize an active state. Further understanding of these specific agonist-induced changes in GPCRs may help to establish a structural basis for the functional selectivity of ligands and benefit the design of better agonist-based pharmaceuticals.

Prior to this study, the examination of a number of different agonists in crystallization trials with different types of GPCRs suggested that agonists increased the dynamics of the receptor leading to poor quality crystal x-ray diffraction. This observation coupled to most previous ligand-bound GPCR structures being determined in inactive state, suggested that it would be difficult to obtain an agonist-bound structure in an active state without additional stabilization by a G-protein or a mimetic. This study now shows that it is possible to obtain agonist-bound structures at high resolution with a careful choice of conformationally selective ligands, such as the agonist UK-432097 that forms an extensive network of ligand-receptor interactions. It appears that agonist binding does not always induce a greater degree of dynamics on the receptor structure. The type of agonists may be broader than previously believed, where some ligands, such as UK-432097, predominately stabilize only one receptor conformation (conformationally selective ligands), while others shift the dynamic equilibrium of multiple receptor conformations (42).

Supplementary Material

Refer to Web version on PubMed Central for supplementary material.

Acknowledgments

This work was supported in part by the PSI:Biology grant U54 GM094618. Additionally, KJ and ZG acknowledge support from the Intramural Research Program of NIDDK, NIH. RCS thanks Dr. Niek Dekker at Astra Zeneca for suggesting the UK-432097 compound for biochemical and structural studies. The authors thank Jeffrey Velasquez for help on molecular biology, Cromwell Cornillez-Ty, Tam Trinh and Kirk Allin for help on baculovirus expression, Ellen Chien and Wei Liu for advice on protein purification and LCP crystallization, Ian Wilson,Mike Hanson, and Ad IJzerman for careful review and scientific feedback on the manuscript, Katya Kadyshevskaya for

assistance with figure preparation and Angela Walker for assistance with manuscript preparation. The authors acknowledge Laura Heitman for A_{2A}AR compounds used in thermal stability studies; Yuan Zheng, The Ohio State University, and Martin Caffrey, Trinity College (Dublin, Ireland), for use of an in meso robot (built with support from the National Institutes of Health [GM075915], the National Science Foundation [IIS0308078], and Science Foundation Ireland [02-IN1-B266]); and Janet Smith, Robert Fischetti and Nukri Sanishvili at the GM/CA-CAT beamline at the Advanced Photon Source, for assistance in development and use of the minibeam and beamtime. The GM/CA-CAT beamline (23-ID) is supported by the National Cancer Institute (Y1-CO-1020) and the National Institute of General Medical Sciences (Y1-GM-1104). RS is a founder and member of the Board of Directors of Receptos, a GPCR structure based drug discovery company. Atomic coordinates and structure factors have been deposited in the Protein Data Bank with the identification code 3QAK.

References and Notes

1. Cherezov V, et al. Science. 2007; 318:1258. [PubMed: 17962520]
2. Rasmussen SG, et al. Nature. 2011; 469:175. [PubMed: 21228869]
3. Rasmussen SG, et al. Nature. 2007; 450:383. [PubMed: 17952055]
4. Rosenbaum DM, et al. Science. 2007; 318:1266. [PubMed: 17962519]
5. Rosenbaum DM, et al. Nature. 2011; 469:236. [PubMed: 21228876]
6. Wacker D, et al. J Am Chem Soc. 2010; 132:11443. [PubMed: 20669948]
7. Hanson MA, et al. Structure. 2008; 16:897. [PubMed: 18547522]
8. Warne T, et al. Nature. 2008; 454:486. [PubMed: 18594507]
9. Warne T, et al. Nature. 2011; 469:241. [PubMed: 21228877]
10. Jaakola VP, et al. Science. 2008; 322:1211. [PubMed: 18832607]
11. Wu B, et al. Science. 2010; 330:1066. [PubMed: 20929726]
12. Chien EY, et al. Science. 2010; 330:1091. [PubMed: 21097933]
13. Park JH, Scheerer P, Hofmann KP, Choe HW, Ernst OP. Nature. Jul 10.2008 454:183. [PubMed: 18563085]
14. Scheerer P, et al. Nature. 2008; 455:497. [PubMed: 18818650]
15. Mantell SJ, et al. Bioorg Med Chem Lett. 2009; 19:4471. [PubMed: 19501510]
16. Fredholm BB, Ijzerman AP, Jacobson KA, Linden J, Muller C. Pharmacol. Rev. 2011; 63:1. [PubMed: 21303899]
17. Rieger JM, Brown ML, Sullivan GW, Linden J, Macdonald TL. J Med Chem. 2001; 44:531. [PubMed: 11170643]
18. Tchilibon S, et al. Bioorg Med Chem. 2004; 12:2021. [PubMed: 15080906]
19. The ligand binding properties of UK-432097 and related nucleosides were examined in membranes from A_{2A}AR-T4L-ΔC-expressing Sf9 cells (Fig. S1). The Ki of UK-432097 at the A_{2A}AR-T4L-ΔC receptor was 4.75 nM. The agonist property of UK-432097 was characterized using CHO cells expressing human WT A_{2A}AR. The efficacy and potency of UK-432097 in comparison to other three known agonists (NECA, CGS21680 and CI-936) were followed using a cylic AMP accumulation assay in intact CHO cells. The EC50 values of UK-432097, NECA, CGS21680 and CI-936 are 0.66 ± 0.19, 5.99 ± 1.86, 3.25 ± 1.22 and 14.5 ± 5.81 nM, respectively (Fig. S2).
20. Gao ZG, Ijzerman AP. Biochem Pharmacol. 2000; 60:669. [PubMed: 10927025]
21. Materials and methods are available as supporting material on *Science* online.
22. To overcome the inherent structural flexibility of GPCRs, we employed the same engineered A_{2A}AR construct, termed A_{2A}AR-T4L-ΔC, as was used in A_{2A}AR/ZM241385 complex structure. Briefly, this construct contains an insertion of T4 lysozyme (T4L) at the intracellular loop 3 (ICL3) and removal of C-terminal 96 residues of A_{2A}AR. Stabilization of the A_{2A}AR-T4L-ΔC construct in an active state was achieved by screening a broad range of A_{2A}AR agonists using a thermal melting CPM assay. Among the tested ligands, UK-432097 exhibited the highest thermal stability (Tm ~65 °C; Table S3). The stabilized A_{2A}AR-T4L-ΔC in complex with UK-432097 was crystallized in a cholesterol-doped monoolein lipidic cubic phase (LCP). Crystallographic data were collected on the GM/CA CAT beamline at the Argonne Photon Source using a 10 μm minibeam. A complete dataset at 2.7 Å resolution was assembled using data collected from 20 crystals. The final model includes residues Ile3 to Leu308 of the human A_{2A}AR, residues 2 to 161 of T4L replacing the ICL3 of A_{2A}AR (Lys209 to Ala221), two partial

lipid (OLC, (2R)-2,3-dihydroxypropyl (9Z)-octadec-9-enoate) chains, 6 water molecules and the agonist UK-432097 bound in the ligand-binding cavity. Part of the extracellular loop 2 (ECL2; Pro149 to Gln157) was not modeled due to a weak electron density.

23. Cristalli G, Muller CE, Volpini R. Handb Exp Pharmacol. 2009:59. [PubMed: 19639279]
24. Ivanov AA, Barak D, Jacobson KA. J Med Chem. 2009; 52:3284. [PubMed: 19402631]
25. Jaakola VP, et al. J Biol Chem. 2010; 285:13032. [PubMed: 20147292]
26. In Ballesteros-Weinstein numbering, a single most conserved residue among the class A GPCRs is designated x.50, where x is the transmembrane helix number. All other residues on that helix are numbered relative to this conserved position.
27. Ballesteros JA, Weinstein H. Meth Neurosci. 1995; 25:366.
28. Kim J, Wess J, van Rhee AM, Schoneberg T, Jacobson KA. J Biol Chem. 1995; 270:13987. [PubMed: 7775460]
29. Jiang Q, Lee BX, Glashofer M, van Rhee AM, Jacobson KA. J Med Chem. 1997; 40:2588. [PubMed: 9258366]
30. Jiang Q, et al. Mol Pharmacol. 1996; 50:512. [PubMed: 8794889]
31. Conn PJ, Christopoulos A, Lindsley CW. Nat Rev Drug Discov. 2009; 8:41. [PubMed: 19116626]
32. Gao ZG, et al. Mol Pharmacol. 2003; 63:1021. [PubMed: 12695530]
33. Katritch V, Kufareva I, Abagyan R. Neuropharmacology. 2011; 60:108. [PubMed: 20637786]
34. Note that global superimposition of TM helical bundle in this case almost exactly overlaps common features of A_{2A}AR/ZM241385 and A_{2A}AR/UK-432097 complexes, so that the Asn253$^{6.55}$ α-carbonyls of A_{2A}AR are within 0.2 Å and exocyclic amines of ZM241385 and UK-432097 are within 0.6 Å distance.
35. Vogel R, Siebert F. J Biol Chem. 2001; 276:38487. [PubMed: 11502747]
36. Hofmann KP, et al. Trends Biochem Sci. 2009; 34:540. [PubMed: 19836958]
37. Sansuk K, et al. Mol Pharmacol. 2011; 79:262. [PubMed: 21081645]
38. Ahuja S, Smith SO. Trends Pharmacol Sci. 2009; 30:494. [PubMed: 19732972]
39. Vanni S, Neri M, Tavernelli I, Rothlisberger U. J Mol Biol. 2010; 397:1339. [PubMed: 20132827]
40. Wess J, Han SJ, Kim SK, Jacobson KA, Li JH. Trends Pharmacol Sci. 2008; 29:616. [PubMed: 18838178]
41. Katritch V, et al. J Mol Recognit. 2009; 22:307. [PubMed: 19353579]
42. Yao XJ, et al. Proc Natl Acad Sci U S A. 2009; 106:9501. [PubMed: 19470481]

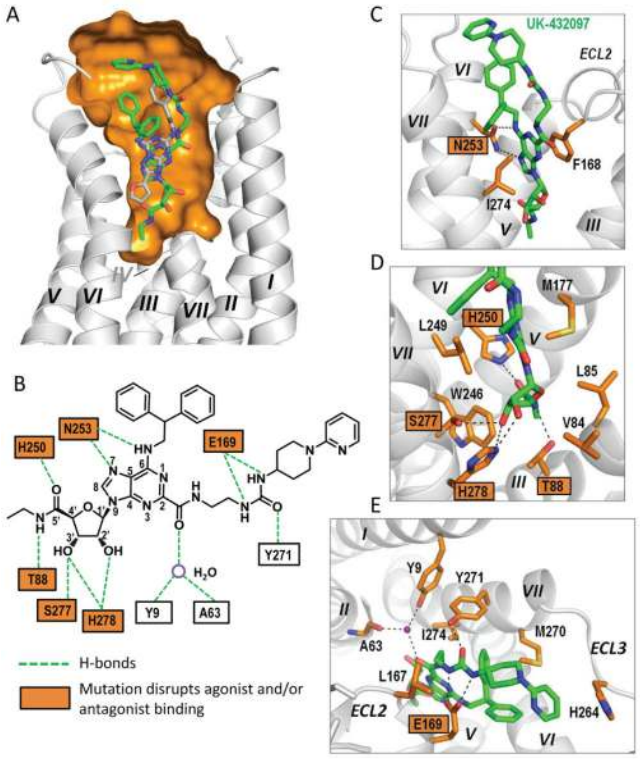

Fig. 1.

Ligand UK-432097 and its binding cavity. (**A**) Overall view of the ligand-binding cavity. The transmembrane part of A_{2A}AR is shown as ribbon and colored gray (helices I to VII). Ligand UK-432097 is shown as bright green stick. For comparison, ligand ZM241385 (gray stick) is also shown at the position when the two complex structures were superimposed. The binding cavity is represented by orange surface (calculated with the program Hollow). Part of helix VII is removed for clarity. (**B**) Schematic representation of the hydrogen-bonding interactions (green dashed lines) between A_{2A}AR and UK-432097. (**C**) Molecular interactions within the ligand-binding cavity for UK-432097 around the adenine moiety. Interacting residues are shown as sticks with side chains colored orange. Hydrogen bonds between A_{2A}AR and ligand are shown as black dotted lines. (**D**) Molecular interactions around the ribose moiety. (**E**) Molecular interactions around the ligand substitution sites. A water molecule is shown as purple sphere. In (B)-(E), residue mutations reported to disrupt agonist and/or antagonist binding are indicated with orange squares. The images were created with PyMOL.

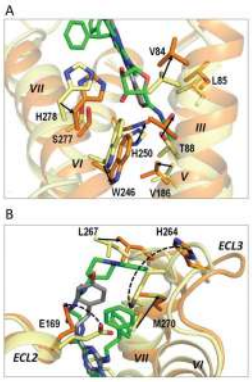

Fig. 2.

Ligand-binding cavity comparison between A_{2A}AR/UK-432097 and A_{2A}AR/ZM241385 complexes. Two receptors were superimposed using Cα atoms of the TM helices. UK-432097 bound A_{2A}AR is colored orange (ribbon) with ligand colored green (stick), ZM241385 bound A_{2A}AR (PDB ID: 3EML) is colored yellow (ribbon) with ligand colored gray (stick). (**A**) Comparison of the binding pocket around the ligand ribose moiety. Deviating residues (with either backbone or side-chain movement) are shown in sticks. The direction of movement is indicated by black arrows. For clarity, only helices III, VI, VII and part of helix V are shown. (**B**) Binding pocket comparison around the substitution part of the ligand. Prominent rotameric switches of Glu169 and His264 on ECL2 and ECL3, respectively, are indicated by dotted black arrows. The images were created with PyMOL.

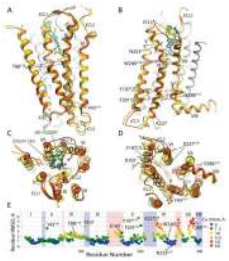

Fig. 3.

Analysis of conformational variations between A_{2A}AR/UK-432097 (orange) and A_{2A}AR/ZM241385 (yellow; PDB ID: 3EML) complexes. Two protein conformations were superimposed using Cα atoms of the TM helices. Heavy atom RMSDs were calculated for each residue of the receptor. (**A**) side view of helices I-IV; (**B**) side view of helices V-VIII; (**C**) extracellular (top) view; (**D**) intracellular (bottom) view. Most pronounced global changes in the TM helices are shown by black arrows. Side chains that change rotamer conformation are shown in sticks. (**E**) Plot showing individual residue deviations between superimposed A_{2A}AR conformations, where each residue dot is also colored by deviation of its Cα atom (blue-green dots with high RMSD thus represent residues with rotamer switches). Regions of intracellular loops and helix VIII in the plot are shaded blue, the extracellular loops shaded pink. The images were created with ICM software (Molsoft LLC). Animated version of this figure can be found in Supporting Online Material.

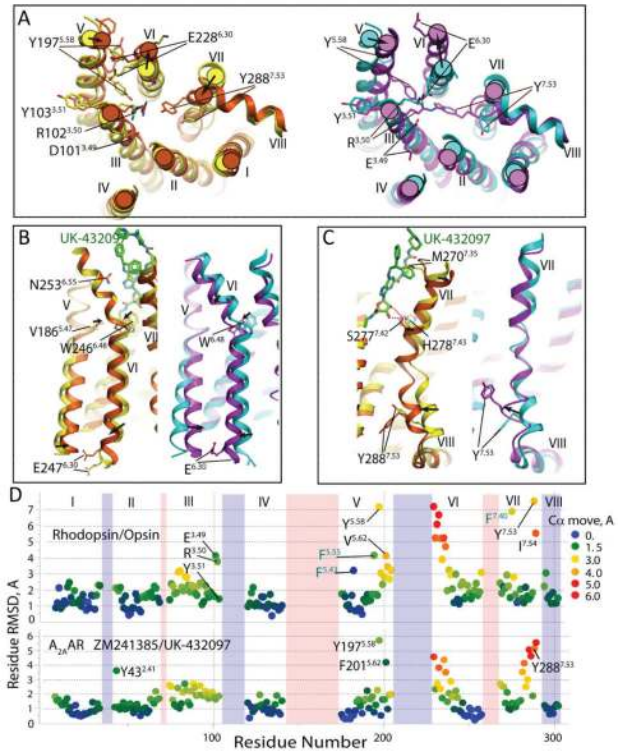

Fig. 4.

Comparison of conformational changes in $A_{2A}AR$ TM bundle between antagonist (yellow; ZM241385 PDB ID: 3EML) and agonist (orange; UK-432097) bound states to conformational changes in rhodopsin between inactive (cyan; PDB ID: 1GZM) and active-like (purple; PDB ID: 3DQB) states. The proteins were superimposed using Cα atoms of the TM helices. Side chains with switches in rotamer state and those critical for agonist interactions are shown in stick presentations. (**A**) Intracellular view on the 7TM helical bundle shown for $A_{2A}AR$ antagonist and agonist bound states on the left panel and for inactive Rhodopsin and active-like opsin on the right panel. (**B**) Comparison of movements in helices V and VI of $A_{2A}AR$ (yellow/orange) and Rho (cyan/purple). (**C**) Same for movements in helix VII. (**D**) Plot compares individual residue deviations in the 7TM bundle for $A_{2A}AR$ and Rhodopsin GPCRs; each residue dot is also colored by deviation of its Cα atom. Intracellular loops and helix VIII regions are shaded blue, extracellular loops shaded pink. The images were created with ICM software (Molsoft LLC).

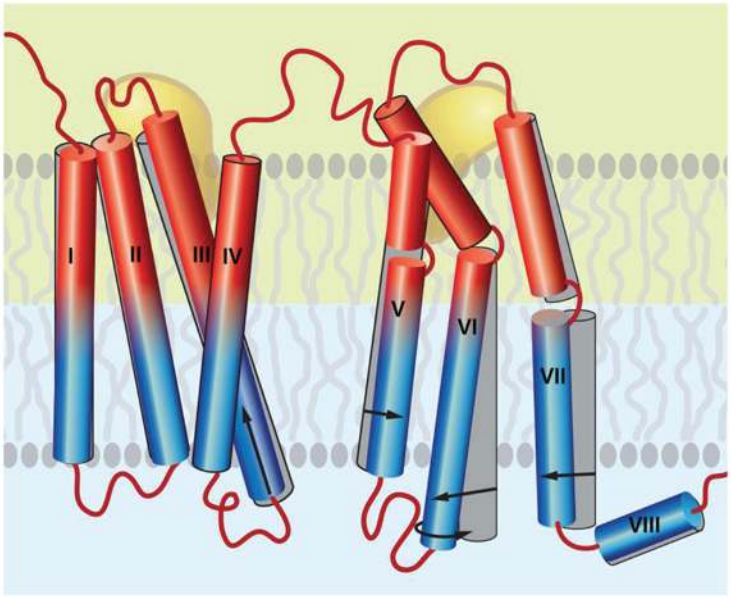

Fig. 5.

Modularity and common features of the activation mechanism in class A GPCRs. Relatively small agonist-specific conformational changes in the extracellular ligand binding module of the receptor (colored red) promote major rearrangements in the intracellular module (colored blue). The major changes include pronounced tilt of the intracellular parts of helices V (inward) and VI (outward), the latter combined with rotation, an inward tilt of the helix VII, as well as an axial shift of helix III. While the magnitude of changes observed in the three receptors, opsin, β_2AR and A_{2A}AR varies, the overall direction of each helix movements and their effect on reshaping of the G-protein binding site are similar. Note modularity between the "core" bundle of helices I-IV that changes the least, and a significantly more mobile module comprising helices V-VII. This architecture is reminiscent of antibodies, where a conserved two-domain framework is combined with complementarity determining regions (CDRs), or CDR loops to recognize a diverse array of molecules.